Low-frequency radiation of a charged particle bunch on a double grid screen

Evgenii S. Simakov,* Andrey V. Tyukhtin, and Sergey N. Galyamin
Faculty of Physics, St. Petersburg State University, St. Petersburg, Russia

(Received 27 November 2025; accepted 18 March 2026; published 17 April 2026)

We analyze the radiation of a charged particle bunch passing through two grids parallel to each other (the double grid screen). The grid is composed of thin conductors that form square cells and have galvanic contact at the cross points. It is assumed that the wavelengths under consideration are much greater than the cell size, and the latter is much greater than the wire thickness. In this approximation, the structure can be described analytically by the averaged boundary conditions. Asymptotic analysis of the electromagnetic field shows that the bunch generates cylindrical and spherical waves. In particular, it is demonstrated that the cylindrical ones are dominant in the area between the grids. It is important to note that the structure under consideration can be practically transparent to a bunch, which is quite promising, in particular, for developing new methods of nondestructive bunch diagnostics.

DOI: 10.1103/33q5-wtc7

I. INTRODUCTION

Studying the radiation of charged particles moving in the presence of periodic structures is crucial for developing such areas of modern science as accelerator and beam physics. As a rule, periodic structures are used to generate the well-known Smith-Purcell radiation (SPR), which is excited at wavelengths comparable to or less than the structure period [1–9]. In particular, SPR is applied in free-electron lasers [6,7] and can be quite useful for nondestructive bunch diagnostics [8,9].

However, charged particles generate electromagnetic radiation not only in the "resonant" spectrum range. Recent studies demonstrate that radiation at long wavelengths (relative to the structure period) is also of significant interest. Here one can mention papers that are devoted to investigating periodic conductive structures such as corrugated ones with a rectangular profile [10–13]. In studies [10,11], it was demonstrated that a charged particle bunch moving inside a corrugated waveguide with a relatively small corrugation period can generate powerful emission in the frequency range corresponding to tenths of THz. In papers [12,13], the authors examined a planar corrugated structure and showed that a bunch moving along the structure excites surface waves whose characteristics can be useful for bunch diagnostics. Note that in [12,13], the analytical solutions were obtained by applying the equivalent boundary conditions [14].

Another common type of periodic structures is a system of thin parallel wires. If the distance between the wires is much smaller than the wavelength and much greater than the thickness of the wires, the structure can be described by the average boundary conditions (ABC) of Kontorovich *et al.* [15]. The ABC method was successfully applied, for example, in papers [16–18], where the infinite and semi-infinite planar structures were studied. Authors examined different variants of bunch motion (with respect to the structure plane) and showed that the bunch generates, in particular, surface waves propagating along the wires. The characteristics of the surface wave allow determining a bunch profile, which is quite interesting for developing new methods of bunch diagnostics.

The ABC method can also be used when thin wires form a grid [15,19,20]. In [19], a system of two parallel grids was proposed as a filter for selective screening of waveguide modes. It was assumed that the wires form square cells and have galvanic contact at the cross points. The authors showed, in particular, that the filter can effectively select a single mode under the condition that its wavelength differs significantly from those of other excited modes. Paper [20] is devoted to the problem of determining the energy of a charged particle bunch moving inside a waveguide. It was demonstrated that the energy can be calculated by using the dependence of a mode frequency on the Lorentz factor. The results of this work illustrate that the proposed method is effective, in particular, when a waveguide wall is the grid with rectangular cells.

The present work aims to investigate the electromagnetic radiation of a charged particle bunch passing through two

*Contact author: e.simakov@spbu.ru

Published by the American Physical Society under the terms of the Creative Commons Attribution 4.0 International license. Further distribution of this work must maintain attribution to the author(s) and the published article's title, journal citation, and DOI.

parallel grids with square cells (the double grid screen). The thickness of the wires, which form the grids and have galvanic contact at the cross points, is assumed to be much less than the cell size. The latter, in turn, is much smaller than the lengths of electromagnetic waves under consideration. In this case, the ABC method is applied, and these conditions are isotropic [15].

It is worth noting that the grid structure composed of thin wires is applied in experiments as a tool for bunch diagnostics. Here one can mention such devices as the secondary electron emission (SEM) grids [21–24], which are designed to determine the transverse profile and emittance of a bunch. The diagnostics is generally invasive and based on measuring electric currents, which are generated in the wires when the bunch particles physically interact with the conductors of the structure.

A series of our works mentioned above proposes to use the structures composed of thin wires in a different way [16–18,20]. We propose measuring an averaged electromagnetic field generated by interaction between the field of a bunch and the periodic system of conductors. It should be noted that a change in the wire thickness has little effect on the averaged properties of the structure since the ABC depends on the logarithm of the ratio of the structure period to the wire thickness. Consequently, the latter can be reduced so that the mechanical interaction between the conductors and the bunch is insignificant. Thus, there is an opportunity to develop a diagnostic technique that is virtually nondestructive to the bunch. In this paper, we study the double grid screen, which allows obtaining intense radiation in the area between the grids.

II. AVERAGED BOUNDARY CONDITIONS AND GENERAL SOLUTION

The structure under consideration is shown in Fig. 1. The grids are located in a vacuum; they are parallel to each other, and the distance between them is h. Each grid is composed of thin conductors, which have galvanic contact at the cross points and form square cells with the side length a. It is assumed that h and the length of an electromagnetic wave, λ, are much greater than a, and the latter is much greater than the transverse size of a conductor, d_0. This results in the inequalities

$$d_0 \ll a \ll \lambda, h. \tag{2.1}$$

If (2.1) are fulfilled, the influence of the grid on an electromagnetic field can be described by the average boundary conditions (ABC) of Kontorovich. The ABC relate the averaged (over the grid cell) Fourier transforms of the electric field $\vec{E}_\omega$ and the surface current density $\vec{I}_\omega$ in accordance with the formula [15]

$$\vec{E}_{\tau\omega} = -i\frac{8\pi k_0 a}{c} A\left(B\vec{I}_\omega + \frac{1}{2k_0^2}\nabla_\tau \mathrm{div}\vec{I}_\omega\right). \tag{2.2}$$

Here $k_0 = \omega/c = 2\pi/\lambda$ is the wave number, ω is the angular frequency, c is the speed of light in a vacuum, and subscript τ denotes the tangential (to the boundary) component of a vector. Note that the relation between the surface current density $\vec{I}_\omega$ and the magnetic field $\vec{H}_\omega$ is written in the form

$$\vec{I}_\omega = \frac{c}{4\pi}[\vec{e}_z, \{\vec{H}_\omega\}], \tag{2.3}$$

where

$$\{\vec{H}_\omega\} = \vec{H}_\omega|_{z=+0} - \vec{H}_\omega|_{z=-0} \tag{2.4}$$

is the jump of the magnetic field in the plane $z = 0$ (likewise for the plane $z = h$). The parameters A and B in (2.2) are determined by the expressions

$$A = \frac{1}{4\pi}\ln\left(\frac{a}{\pi d_0}\right), \qquad B = 1 + \frac{\mu_i f(p)}{4\ln[a/(\pi d_0)]}. \tag{2.5}$$

Here μ_i is the magnetic permeability of the conductors, and function $f(p)$ has a simple form in the following particular cases

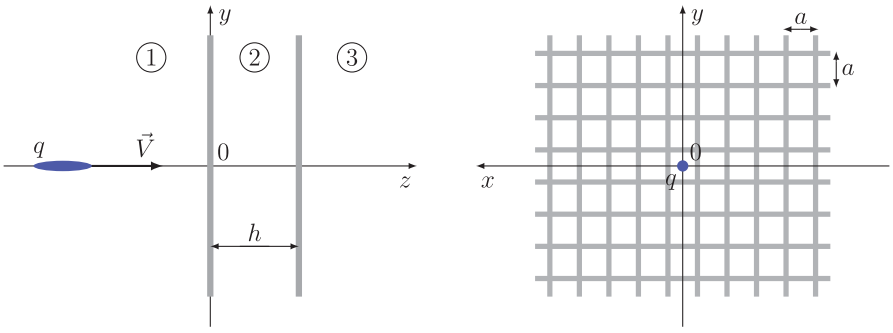


FIG. 1. Double grid screen and a moving bunch. Plane (y, z) is on the left, plane (x, y) is on the right.

$$f(p) = \begin{cases} -i + 1/p^2, & p \ll 1 \\ (1-i)/p, & p \gg 1 \end{cases}, \tag{2.6}$$

where $p = d_0/(4d_s)$, d_s is the skin depth. It should be noted that, at frequencies in the GHz range, the skin depth of metals does not exceed a few microns. Taking this fact into account, we will consider only the case when $p \gg 1$. Under this condition, one can neglect the finite conductivity of the wires and assume that $B = 1$.

It is assumed that a charged particle bunch moves along z axis with the constant velocity $\vec{V} = V\vec{e}_z$ (see Fig. 1). The bunch has an infinitesimal transverse size and arbitrary charge distribution along the trajectory of motion, i.e., its charge and current densities can be written in the form

$$\rho = q\delta(x)\delta(y)\varkappa(\zeta), \qquad j_z \equiv j = \rho V. \tag{2.7}$$

Here $\zeta = z - Vt$, q is the total charge of the bunch, δ is the Dirac delta-function, and $\varkappa(\zeta)$ is the bunch profile (the longitudinal charge distribution). Note that $\int_{-\infty}^{+\infty} \varkappa(\zeta)d\zeta = 1$.

Let us use Hertz potential and present it as a sum of "forced" and "free" ones. The former characterizes an electromagnetic field of the bunch in an unbounded vacuum, and the latter characterizes an electromagnetic field caused by an influence of the grids. Note that the terms "forced" and "free" were used by Ginzburg and Tsytovich in [25].

The "forced" Hertz potential satisfies the inhomogeneous Helmholtz equation and describes the well-known Coulomb field of the charge in an unbounded vacuum. In the cylindrical coordinates, the Fourier transform of this potential is $\Pi^{(i)}_{r\omega} = \Pi^{(i)}_{\varphi\omega} = 0$,

$$\Pi^{(i)}_{z\omega} = \frac{iq\tilde{\varkappa}}{ck_0}\exp(ik_0 z/\beta)\int_{-\infty}^{+\infty}\frac{k_r H_0^{(1)}(k_0 k_r r)}{k_r^2 + (1-\beta^2)/\beta^2}dk_r, \tag{2.8}$$

where $H_0^{(1)}$ is the Hankel function, $\beta = V/c$, k_r is the dimensionless transverse component of a wave vector, and function

$$\tilde{\varkappa} = \frac{1}{2\pi}\int_{-\infty}^{+\infty}\varkappa(\zeta)\exp(-ik_0\zeta/\beta)\,d\zeta \tag{2.9}$$

is the Fourier transform of the bunch profile $\varkappa(\zeta)$.

The "free" Hertz potential satisfies the homogeneous Helmholtz equation. Let us introduce the Hertz potentials $\vec{\Pi}^{(1)}$, $\vec{\Pi}^{(2)}$, and $\vec{\Pi}^{(3)}$, which refer to the areas $z < 0$, $0 < z < h$, and $z > h$, respectively (these areas are denoted by 1, 2, and 3 in Fig. 1). Their Fourier transforms can be written in the following way

$$\begin{Bmatrix} \Pi^{(1)}_{z\omega} \\ \Pi^{(3)}_{z\omega} \end{Bmatrix} = \frac{iq\tilde{\varkappa}\beta}{ck_0}\int_{-\infty}^{+\infty}\begin{Bmatrix} T_1 \\ T_3 \end{Bmatrix}\frac{k_r H_0^{(1)}(k_0 k_r r)}{1-\beta^2 k_z^2}\exp(ik_0 k_z|z|)dk_r, \tag{2.10}$$

$$\Pi^{(2)}_{z\omega} = \frac{iq\tilde{\varkappa}\beta}{ck_0}\int_{-\infty}^{+\infty}\frac{k_r H_0^{(1)}(k_0 k_r r)}{1-\beta^2 k_z^2}[T_{21}\exp(ik_0 k_z z) + T_{22}\exp(-ik_0 k_z z)]dk_r. \tag{2.11}$$

Other components of the Hertz potentials are equal to zero. In (2.10) and (2.11), the coefficients T_1, T_{21}, T_{22}, T_3 are unknown and can be determined by using the averaged boundary conditions. Note that $k_z = \sqrt{1-k_r^2}$ is the dimensionless longitudinal component of the wave vector. This function should be defined as follows. If $k_r^2 < 1$, k_z is purely real and positive, which is explained by the fact that the waves of the three-field propagate away from the structure. If $k_r^2 > 1$, k_z is purely imaginary, and $\mathrm{Im}k_z > 0$. In this case, the magnitude of a wave decreases exponentially with an increase of z.

To find the Fourier transforms of electromagnetic field components, we use the relations

$$\vec{E}_\omega = \nabla \mathrm{div}\vec{\Pi}_\omega + k_0^2\vec{\Pi}_\omega, \qquad \vec{H}_\omega = -ik_0 \mathrm{rot}\vec{\Pi}_\omega. \tag{2.12}$$

Then, utilizing the total electromagnetic field, we apply boundary conditions (2.2) at $z = 0$ and $z = h$, solve the corresponding 4×4 linear system and obtain the expressions for the coefficients. Omitting the intermediate calculations, we present the results

$$T_1 = \frac{k_z[1+\exp(i\xi)] - g[\exp(i\xi)+\exp(i\psi)]}{k_z^2 - g^2\exp(i\psi)}, \tag{2.13}$$

$$T_{22} \equiv T_2 = \frac{k_z - g\exp(i\xi)}{k_z^2 - g^2\exp(i\psi)}, \qquad T_{21} = T_2 - T_1, \tag{2.14}$$

$$T_3 = \frac{g[1+\exp(i\xi)]\exp(i\psi) - k_z[\exp(i\xi)+\exp(i\psi)]}{k_z^2 - g^2\exp(i\psi)}, \tag{2.15}$$

where

$$g = k_z - 2ik_0 h\alpha A(1+k_z^2),$$
$$\psi = -2k_0 h k_z,\ \ \xi = k_0 h(1-\beta k_z)/\beta. \tag{2.16}$$

Note that the expression for g contains $\alpha = a/h$, which is, according to (2.1), the small parameter of the problem.

III. ASYMPTOTIC ANALYSIS

Below, we present the asymptotic analysis of integrals (2.10) and (2.11). Note that we consider only the positive frequencies ($k_0 = \omega/c > 0$). Corresponding expressions for the negative ones ($k_0 = \omega/c < 0$) can be derived by the rule $F_{-\omega} = F_{\omega}^*$, where the asterisk means complex conjugation.

Assuming that $k_0 k_r r \gg 1$, we take into account the asymptotic expansion for the Hankel function $H_0^{(1)}(k_0 k_r r)$ and, according to the second formula in (2.14), obtain

$$\begin{Bmatrix} \Pi_{z\omega}^{(1)} \\ \Pi_{z\omega}^{(3)} \end{Bmatrix} \simeq \frac{(1+i)q\tilde{\varkappa}\beta}{ck_0\sqrt{\pi k_0 r}} \int_{-\infty}^{+\infty} \begin{Bmatrix} T_1 \\ T_3 \end{Bmatrix} \frac{\sqrt{k_r}}{1-\beta^2 k_z^2} \exp\left[ik_0(k_r r + k_z|z|)\right] dk_r, \tag{3.1}$$

$$\Pi_{z\omega}^{(2)} \simeq -\Pi_{z\omega}^{(1)} + \frac{2(1+i)q\tilde{\varkappa}\beta}{ck_0\sqrt{\pi k_0 r}} \int_{-\infty}^{+\infty} T_2 \frac{\sqrt{k_r}}{1-\beta^2 k_z^2} \cos(k_0 k_z z) \exp(ik_0 k_r r) dk_r. \tag{3.2}$$

The integrands in (3.1) and (3.2) have a series of singularities. They can be found from the dispersion equation

$$(1-\beta^2 k_z^2)[k_z^2 - g^2 \exp(-2ik_0 h k_z)] = 0, \tag{3.3}$$

where the expression in the square brackets is the denominator of T_1, T_2, and T_3. We note again that $k_z = \sqrt{1-k_r^2}$.

The solutions of the equation

$$1 - \beta^2 k_z^2 = 0 \tag{3.4}$$

are $k_r = \pm k_r^{(i)} = \pm i\sqrt{1-\beta^2}/\beta$. As will be shown, only pole $+k_r^{(i)}$ contributes to the integrals (3.1) and (3.2). However, the pole is purely imaginary; its contribution results in the exponential decrease of the field magnitude with an increase of r and can be neglected under the condition $k_0 r\sqrt{1-\beta^2}/\beta \gg 1$.

One more equation that follows from (3.3) is

$$k_z^2 - g^2 \exp(-2ik_0 h k_z) = 0, \tag{3.5}$$

where g is determined by the first formula in (2.16). In the linear approximation relative to the small parameter $\alpha = a/h$, (3.5) transforms into the equation

$$1 - \exp(-2ik_0 h k_z) = -\frac{4ik_0 h\alpha A}{k_z}(1+k_z^2)\exp(-2ik_0 k_z h), \tag{3.6}$$

which has the following approximate solutions

$$k_z = k_{zm} = k_{zm}^{(0)} + k_{zm}^{(1)}, \qquad k_{zm}^{(1)} = -\frac{2\alpha A}{k_{zm}^{(0)}}\left[1 + (k_{zm}^{(0)})^2\right]. \tag{3.7}$$

Here

$$k_{zm}^{(0)} = \frac{m}{M}, \qquad m \in \mathbb{N}, \tag{3.8}$$

and the parameter

$$M = \frac{k_0 h}{\pi} = \frac{\omega h}{c\pi} = \frac{h}{(\lambda/2)}. \tag{3.9}$$

Note that, in particular, M indicates the number of half-wavelengths between the grids. Thus, the poles of the integrands in (3.1) and (3.2) are determined by the expressions

$$k_r = \pm k_{rm} = \pm(k_{rm}^{(0)} + k_{rm}^{(1)}), \qquad k_{rm}^{(1)} = \frac{2\alpha A}{k_{rm}^{(0)}}\left[1 + (k_{zm}^{(0)})^2\right], \tag{3.10}$$

where

$$k_{rm}^{(0)} = \sqrt{1 - (k_{zm}^{(0)})^2} = \sqrt{1 - \frac{m^2}{M^2}}. \tag{3.11}$$

It should be emphasized that expressions (3.10) are valid when $m \neq M$. Otherwise, we have

$$k_r = \pm k_{rM} = \pm 2\sqrt{2\alpha A}. \tag{3.12}$$

Further, we will consider only the case when $m \leq M$. Under this condition, the poles are purely real, and their contributions to the integrals (3.1) and (3.2) are propagating waves.

The asymptotic investigation of the integrals is carried out by the use of the saddle point method, which can be applied under the conditions $k_0 R \gg 1$ and $\theta \gg 1/\sqrt{k_0 R}$, where $R = \sqrt{r^2 + z^2}$ and θ is the angle of the spherical coordinate system. It is convenient to introduce the new integration variable χ by the rule

$$k_r = \sin\chi. \tag{3.13}$$

The saddle point is the solution of the equation $\partial\Phi(\chi)/\partial\chi = 0$, where $\Phi(\chi) = \cos(\chi - \theta)$ is the phase function. It is easy to show that the saddle point is the angle θ. The steepest descent path Γ^* contains point θ and can be found from the system

$$\begin{aligned} &\mathrm{Im}\,\Phi(\chi) > \mathrm{Im}\,\Phi(\theta) \\ &\mathrm{Re}\,\Phi(\chi) = \mathrm{Re}\,\Phi(\theta)\ . \end{aligned} \tag{3.14}$$

As follows from (3.14), Γ^* satisfies the equation

$$\mathrm{ch}\chi'' = \frac{1}{\cos(\theta - \chi')}, \tag{3.15}$$

where $\theta - \pi/2 < \chi' < \theta$, if $\chi'' > 0$, and $\theta < \chi' < \theta + \pi/2$, if $\chi'' < 0$. Note that expression (3.2) is determined as well by the integral containing the phase function $\Phi(\chi) = -\cos(\chi + \theta)$. In this case, the saddle point is $\pi - \theta$, and the steepest descent path satisfies the equation

$$\mathrm{ch}\chi'' = -\frac{1}{\cos(\theta + \chi')}, \tag{3.16}$$

where $\pi/2 - \theta < \chi' < \pi - \theta$, if $\chi'' > 0$, and $\pi - \theta < \chi' < 3\pi/2 - \theta$, if $\chi'' < 0$.

The location of the poles $\pm\chi_m$ $(m = 1, 2, \ldots)$ and $\pm\chi^{(i)}$, the angle θ (denoted by the gray point), the integration path Γ, and the steepest descent path Γ^* in the complex plane χ is illustrated in Fig. 2. The poles $\pm\chi_m$ and $\pm\chi^{(i)}$ correspond to $\pm k_{rm}$ and $\pm k_r^{(i)}$, respectively. Such location of the poles relative to the integration path can be obtained if we take into account negligibly small attenuation in the medium. According to Fig. 2, only the poles $+k_{rm}$ and $+k_r^{(i)}$ can contribute to the integrals (3.1) and (3.2). As was mentioned above, the contribution of $+k_r^{(i)}$ is not of interest because it is not the radiation field.

As follows from (3.10)–(3.12), the poles $+k_{rm}$ are purely real under the condition $m \leq M$. In this case, their contributions are cylindrical waves. If $m > M$, the poles are purely imaginary and not of interest to us. As is clear from Fig. 2, the pole with the number m contributes to the integrals when θ is greater than certain angle θ_m. According to formulas (3.8), (3.10), (3.11), and (3.13), this inequality can be written in the form

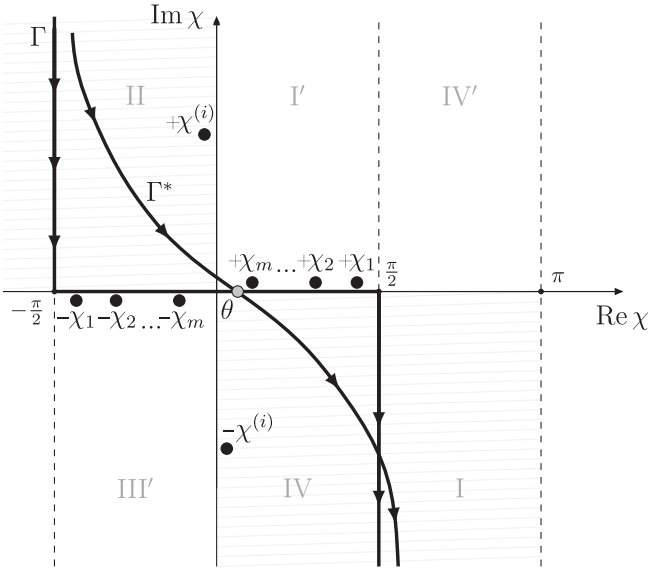


FIG. 2. Location of the poles $\pm\chi_m$ $(m = 1, 2, 3\ldots)$ and $\pm\chi^{(i)}$, the angle θ (denoted by the gray point), the integration path Γ, and the steepest descent path Γ^* in the complex plane χ. The roman numerals denote the areas corresponding to the quadrants of the plane k_r (for the "upper" sheet—without a stroke, for the "lower" sheet—with a stroke).

$$\theta > \theta_m = \arcsin\left[\sqrt{1 - \frac{m^2}{M^2}}\left(1 + 2\alpha A\frac{M^2 + m^2}{M^2 - m^2}\right)\right], \tag{3.17}$$

where $m < M$. If $m = M$, the pole is determined by (3.12), and we obtain

$$\theta > \theta_M = \arcsin\left(2\sqrt{2\alpha A}\right) \simeq 2\sqrt{2\alpha A}. \tag{3.18}$$

It should be emphasized that, in the far-field zone, the area $0 < z < h$ (between the grids, see Fig. 1) is characterized by only $\theta = \pi/2$, which corresponds the direction along the grid plane. In this case, the contributions of all the real poles have to be taken into account. In the areas $z < 0$ and $z > h$, the range of angles, where the contribution of the pole k_{rm} exists, is from θ_m to $\pi/2$.

The dependence of θ_m on the parameter M is shown in Fig. 3. The solid black, dotted red, and dashed blue curves correspond to the poles $+k_{r1}$, $+k_{r2}$, and $+k_{r3}$, respectively. The calculations were carried out by using formula (3.17) for the grid parameters $a = 0.1$ cm, $d_0 = 0.1$ mm. The small parameter of the problem was assumed to be $\alpha = 0.01$. Therefore, the distance between the grids is constant and equal to $h = a/\alpha = 10$ cm. In this case, as expressions (3.9) show, the value of M varies by a change in

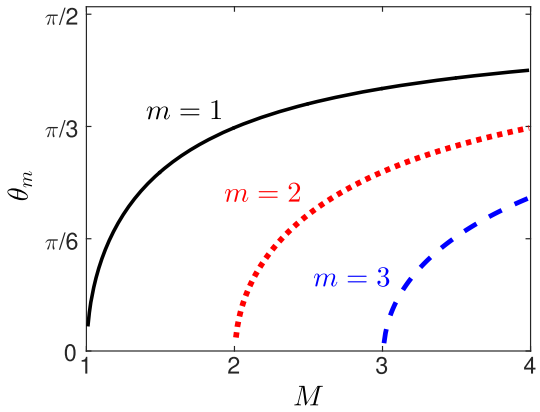


FIG. 3. Dependence of the angle θ_m on the parameter M ($m < M$). The solid black, dotted red, and dashed blue curves correspond to $m = 1, 2$, and 3, respectively. The distance between the grids $h = 10$ cm, the grid period $a = 0.1$ cm, the diameter of the conductors $d_0 = 0.1$ mm.

the wavelength λ. Figure 3 demonstrates that the angle θ_m increases with an increase of M and a decrease of m. If M is slightly greater than m, the pole $+k_{rm}$ contributes to the integrals in the wide range of the angles θ (except the direction close to the trajectory of the bunch motion). A further increase of M leads to narrowing of the range, but the value of the angle θ_m increases more slowly.

In this section, we have demonstrated that, in the far-field zone, integrals (3.1) and (3.2) are determined by the contributions of the poles and the saddle point. Below, we will analyze these contributions separately.

IV. SPHERICAL WAVES

The contribution of the saddle point to the integrals (3.1) and (3.2) can be calculated by the standard formula [26]. Assuming that $k_0R \gg 1$ and $\theta \gg 1/\sqrt{k_0R}$ and using the spherical coordinates, we obtain the following expressions for the areas $z < 0$ and $z > h$

$$\begin{Bmatrix} \Pi^{(1s)}_{R\omega} \\ \Pi^{(3s)}_{R\omega} \end{Bmatrix} = \cos\theta \begin{Bmatrix} \Pi^{(1s)}_{z\omega} \\ \Pi^{(3s)}_{z\omega} \end{Bmatrix}, \quad \begin{Bmatrix} \Pi^{(1s)}_{\theta\omega} \\ \Pi^{(3s)}_{\theta\omega} \end{Bmatrix} = -\sin\theta \begin{Bmatrix} \Pi^{(1s)}_{z\omega} \\ \Pi^{(3s)}_{z\omega} \end{Bmatrix}, \tag{4.1}$$

where

$$\begin{Bmatrix} \Pi^{(1s)}_{z\omega} \\ \Pi^{(3s)}_{z\omega} \end{Bmatrix} \simeq -\frac{2q\tilde{\varkappa}\beta}{ck_0^2(1-\beta^2\cos^2\theta)} \frac{1}{S} \begin{Bmatrix} S_1 \\ S_3 \end{Bmatrix} \frac{\exp(ik_0R)}{R}. \tag{4.2}$$

Here the coefficients S, S_1, S_3 are determined by the formulas

$$S = |\cos\theta|[1-\exp(i\psi)] + 4\pi iM\alpha A(1+\cos^2\theta)\exp(i\psi), \tag{4.3}$$

$$S_1 = |\cos\theta|[1-\exp(i\psi)] + 2\pi iM\alpha A(1+\cos^2\theta)[\exp(i\xi)+\exp(i\psi)], \tag{4.4}$$

$$S_3 = |\cos\theta|\exp(i\xi)[1-\exp(i\psi)] + 2\pi iM\alpha A(1+\cos^2\theta)\exp(i\psi)[1+\exp(i\xi)], \tag{4.5}$$

where

$$\psi = -2\pi M|\cos\theta|, \qquad \xi = \pi M(1-\beta|\cos\theta|)/\beta. \tag{4.6}$$

The relation between an electromagnetic field and the Hertz potential is given by Eq. (2.12). We obtain the expressions

$$\begin{Bmatrix} E^{(1s)}_{\theta\omega} \\ E^{(3s)}_{\theta\omega} \end{Bmatrix} \simeq \begin{Bmatrix} H^{(1s)}_{\varphi\omega} \\ H^{(3s)}_{\varphi\omega} \end{Bmatrix} \simeq \frac{2q\tilde{\varkappa}\beta}{c} \frac{\sin\theta}{1-\beta^2\cos^2\theta} \frac{1}{S} \begin{Bmatrix} S_1 \\ S_3 \end{Bmatrix} \frac{\exp(ik_0R)}{R}, \tag{4.7}$$

which describe the Fourier transform of the electromagnetic field (spherical waves) generated in the areas $z < 0$ and $z > h$ by the bunch passing through the double grid screen. Note that formulas (4.7) were obtained in the linear approximation relative to the small parameter α.

It should be emphasized that, if α tends to zero, expressions (4.7) transform to the well-known formulas for the case of the single ideal screen [25]. In this situation, coefficients (4.3)–(4.5) are greatly simplified, and we have

$$S = S_1 = |\cos\theta|[1-\exp(i\psi)], \qquad S_3 = S\exp(i\xi). \tag{4.8}$$

As one can see, the field components in the areas $z < 0$ and $z > h$ differ by the factor $\exp(i\xi)$. This is due to the fact that the single ideal screens are located at the distance h from each other. If $h = 0$, we obtain $\exp(i\xi) = 1$.

In the area between the grid structures ($0 < z < h$), we assume that $\theta \simeq \pi/2$, and therefore, $r \simeq R$. Under the condition $k_0R \gg 1$, the contribution of the saddle point to the integral (3.2) is determined by [26]

$$\Pi^{(2s)}_{\theta\omega} \simeq -\Pi^{(2s)}_{z\omega} \simeq -\frac{q\tilde{\varkappa}\beta}{ck_0^2}[1+\exp(i\pi M/\beta)]\frac{\exp(ik_0R)}{R}. \tag{4.9}$$

The corresponding field components are

$$E^{(2s)}_{\theta\omega} \simeq H^{(2s)}_{\varphi\omega} \simeq -\frac{q\tilde{\varkappa}\beta}{c}[1+\exp(i\pi M/\beta)]\frac{\exp(ik_0R)}{R}. \tag{4.10}$$

Expressions (4.10) describe the Fourier transform of the electromagnetic field (spherical waves) generated by the bunch in the area between the grids. We note that, in the linear approximation relative to the small parameter $\alpha = a/h$, the formula does not depend on the grid parameters: the period a and the diameter of the conductors, d_0. It should also be added that, as follows from (4.10), the field components are equal to zero under the condition $M = \beta(2l+1)$, where $l = 0, 1, 2\ldots$.

V. CYLINDRICAL WAVES

In this section, we will study the contributions of the poles to the integrals (3.1) and (3.2). We note again that the longitudinal wave numbers k_{zm} and transverse ones $+k_{rm}$ (the poles) are defined by Eqs. (3.7) and (3.10), respectively. In these formulas, $k_{zm}^{(1)}$ and $k_{rm}^{(1)}$ are the small corrections (proportional to α) to the main terms $k_{zm}^{(0)}$ and $k_{rm}^{(0)}$, which are given by (3.8) and (3.11). As was mentioned above, the contributions of the poles are propagating waves under condition that the values of $+k_{rm}$ ($m \in \mathbb{N}$) are purely real, i.e., when $m \le M$.

Calculating the residues, we obtain the following Hertz potentials in the far-field zone

$$\Pi_{z\omega}^{(1c)} \simeq \Pi_{z\omega}^{(3c)} \simeq \sqrt{\pi}\frac{(1-i)q\tilde{\varkappa}\beta}{ck_0\sqrt{k_0 r}} \times \sum_{m<M} \frac{k_{zm}^{(1)}[1-(-1)^m \exp(i\pi M/\beta)]}{\sqrt{k_{rm}^{(0)}}[1-\beta^2(k_{zm}^{(0)})^2]} \times \exp[ik_0(k_{rm}r + k_{zm}|z|)], \tag{5.1}$$

$$\Pi_{z\omega}^{(2c)} \simeq -\Pi_{z\omega}^{(1c)} - 2\frac{(1+i)q\tilde{\varkappa}\beta}{ck_0\sqrt{\pi k_0 r}} \times \sum_{m<M} \frac{k_{zm}[1-(-1)^m \exp(i\pi M/\beta)]}{m\sqrt{k_{rm}}(1-\beta^2 k_{zm}^2)[1-4\alpha A(k_{zm}^{(0)})^{-2}]} \times \exp(ik_0 k_{rm} r)\cos(k_0 k_{zm} z). \tag{5.2}$$

The field components are calculated by the use of relations (2.12). In the areas $z < 0$ and $z > h$, we have

$$\begin{Bmatrix} E_{r\omega}^{(1c)} \\ E_{z\omega}^{(1c)} \\ H_{\varphi\omega}^{(1c)} \end{Bmatrix} \simeq \begin{Bmatrix} -E_{r\omega}^{(3c)} \\ E_{z\omega}^{(3c)} \\ H_{\varphi\omega}^{(3c)} \end{Bmatrix} \simeq \frac{(1-i)q\tilde{\varkappa}\beta\sqrt{\pi k_0}}{c\sqrt{r}} \sum_{m<M} \begin{Bmatrix} k_{zm}^{(0)} \\ k_{rm}^{(0)} \\ -1 \end{Bmatrix} \mathcal{E}_m^{(1,3)}, \tag{5.3}$$

where

$$\mathcal{E}_m^{(1,3)} = \frac{k_{zm}^{(1)}\sqrt{k_{rm}^{(0)}}}{1-\beta^2(k_{zm}^{(0)})^2}[1-(-1)^m \exp(i\pi M/\beta)] \times \exp[ik_0(k_{rm}r + k_{zm}|z|)]. \tag{5.4}$$

In the area $0 < z < h$, the field components are

$$E_{r\omega}^{(2c)} \simeq -E_{r\omega}^{(1c)} - 2\frac{(1-i)q\tilde{\varkappa}\beta\sqrt{k_0}}{c\sqrt{\pi r}} \sum_{m<M} k_{zm}\mathcal{E}_m^{(2)} \sin(k_0 k_{zm} z), \tag{5.5}$$

$$\begin{Bmatrix} E_{z\omega}^{(2c)} \\ H_{\varphi\omega}^{(2c)} \end{Bmatrix} \simeq -\begin{Bmatrix} E_{z\omega}^{(1c)} \\ H_{\varphi\omega}^{(1c)} \end{Bmatrix} - 2\frac{(1+i)q\tilde{\varkappa}\beta\sqrt{k_0}}{c\sqrt{\pi r}} \times \sum_{m<M} \begin{Bmatrix} k_{rm} \\ -1 \end{Bmatrix} \mathcal{E}_m^{(2)} \cos(k_0 k_{zm} z), \tag{5.6}$$

where

$$\mathcal{E}_m^{(2)} = \frac{k_{zm}\sqrt{k_{rm}}}{m(1-\beta^2 k_{zm}^2)[1-4\alpha A(k_{zm}^{(0)})^{-2}]} \times [1-(-1)^m \exp(i\pi M/\beta)]\exp(ik_0 k_{rm} r). \tag{5.7}$$

Formulas (5.3)–(5.7) describe the Fourier transform of the electromagnetic field (cylindrical waves) generated by the bunch passing through the double grid screen. We note again that they were obtained in the linear approximation relative to α. As one can see, the number of propagating waves depends on the value of M, i.e., the number of half-wavelengths between the grids. It should also be mentioned that, in the areas $z < 0$ and $z > h$, the field components are proportional to the small parameter of the problem [$k_{zm}^{(1)} \propto \alpha$, see Eq. (3.7)], whereas the main terms of (5.5) and (5.6) are proportional to α^0.

We emphasize that the field components of the cylindrical waves diminish with distance as $1/\sqrt{r}$. For the spherical waves, according to formulas (4.7) and (4.10), we have a decrease as $1/R$. Thus, in the area between the grids, the cylindrical waves are dominant. However, outside this area, the field components are small and can be comparable to those of the spherical waves only at a relatively large distances from the origin.

The electromagnetic field of the cylindrical waves can be obtained by calculating the corresponding Fourier integrals. Due to the fact that only positive frequencies are considered ($\omega > 0$), the Fourier integral can be written over the positive semiaxis, which results in

$$F = 2\int_0^{+\infty} \mathrm{Re}[F_\omega \exp(-i\omega t)]\,\mathrm{d}\omega. \tag{5.8}$$

For simplicity, we will consider the zeroth approximation relative to the small parameter α, i.e., we will assume

that $\alpha = 0$. In this case, the cylindrical waves are excited only in the area $0 < z < h$. In particular, as follows from (5.6), the z component of the electric field is determined by the expression

$$E_z^{(2c)} = 2\int_{\pi c/h}^{\omega_{\max}} \mathrm{Re}[E_{z\omega}^{(2c)} \exp(-i\omega t)]\, \mathrm{d}\omega = \int_1^{M_{\max}} \tilde{E}_{z\omega}^{(2c)}\, \mathrm{d}M, \tag{5.9}$$

where the integrand

$$\tilde{E}_{z\omega}^{(2c)} = \frac{2\pi c}{h}\mathrm{Re}[E_{z\omega}^{(2c)} \exp(-i\omega t)] = -\mathrm{Re}\left\{\frac{4\pi(1+i)q\tilde{\varkappa}\beta}{\sqrt{r}h^{3/2}} \sum_{m<M} \frac{(M^2-m^2)^{3/4}}{M^2-m^2\beta^2} \times[1-(-1)^m \exp(i\pi M/\beta)]\cos(\pi m z/h) \times \exp[i(\sqrt{M^2-m^2}r - Mct)\pi/h]\right\}. \tag{5.10}$$

We note again that the bunch generates the cylindrical wave with the number $m \in \mathbb{N}$, if $m < M$, where M is defined by (3.9). In (5.9), the lower limit of integration $M = 1$ (or $\omega = \pi c/h$) is explained by the fact that the cylindrical waves are not generated, if $M < 1$. The upper limit $M = M_{\max}$ (or $\omega = \omega_{\max}$) is chosen so that the integrand is relatively small, if $M > M_{\max}$.

It should be emphasized that (5.10) depends on the Fourier transform of the longitudinal bunch profile, $\tilde{\varkappa}$, which is determined by (2.9) and, in general, dependent on M. We will study bunches with the Gaussian and "rectangular" charge distribution, i.e.,

$$\varkappa_{\mathrm{gaus}}(\zeta) = \frac{\exp[-\zeta^2/(2\sigma^2)]}{\sqrt{2\pi}\sigma}, \qquad \varkappa_{\mathrm{rect}}(\zeta) = \frac{\Theta(\sigma - |\zeta|)}{2\sigma}, \tag{5.11}$$

where σ is the half-bunch length, and Θ is the Heaviside step function. According to (2.9) and (3.9), the corresponding Fourier transforms are

$$\tilde{\varkappa}_{\mathrm{gaus}} = \frac{1}{2\pi}\exp[-\pi^2\sigma^2 M^2/(2\beta^2 h^2)], \tag{5.12}$$

$$\tilde{\varkappa}_{\mathrm{rect}} = \frac{1}{2\pi}\frac{\sin[\pi\sigma M/(\beta h)]}{\pi\sigma M/(\beta h)}. \tag{5.13}$$

Figure 4 demonstrates the results of numerical calculations of formulas (5.9) and (5.10). The left column presents the dependence of the integrand $\tilde{E}_{z\omega}^{(2c)}$ on the integration variable M. The middle and right columns present the dependence of the component $E_z^{(2c)}$ on the distance r. The calculations were carried out for the Gaussian bunch with $2\sigma = 0.3$ cm (the top row) and $2\sigma = 0.7$ cm (the middle row) as well as for the "rectangular" bunch with $2\sigma = 1$ cm (the bottom row). As is clear from the left column, the value of $M_{\max}$ depends significantly on the length of the bunch and its shape. For example, if the Gaussian bunch has the length $2\sigma = 0.3$ cm, the integrand $\tilde{E}_{z\omega}^{(2c)}$ is relatively small when $M > M_{\max} \simeq 25$ (the left graph in the top row). Note that the value of $M_{\max}$ and, therefore, a number of the excited modes can be decreased by an increase of the bunch length. As follows from the middle column of Fig. 4, the cylindrical waves form the radiation field consisting of the impulses whose structure can be used for determining the length and shape of the bunch. In the case of the Gaussian bunch, its length can be determined, in particular, by measuring the width of the first impulse. This is clear from the right graphs in the top and middle rows, where the impulses are given on a larger scale. The gray horizontal line shows the maximum value of $E_z^{(2c)}$ (the impulse magnitude) divided by $\sqrt{2}$, and the bunch length is approximately equal to the distance between two gray vertical lines. The results of the calculations carried out for the "rectangular" bunch demonstrate that its length and shape can be determined as well. However, the measurements are less accurate in comparison with the case of the Gaussian bunch. This can be explained by the fact that the form-factor $\tilde{\varkappa}_{\mathrm{rect}}$ and, therefore, the integrand $\tilde{E}_{z\omega}^{(2c)}$ decrease more slowly with an increase of M (this is clear from the left graph in the bottom row). Thus, the selected number of the excited modes is insufficient, and the upper limit of integration in (5.9) has to be increased.

We note again that we analyze the so-called "longwave" approximation, i.e., the radiation at the wavelengths which are much greater than the cell size of the grids. The frequencies corresponding to the well-known Smith-Purcell radiation are not considered in this study. In particular, these "resonant" frequencies can be suppressed in the case when the bunch length is relatively large compared to the structure period. For example, the Gaussian bunch with the length $2\sigma = 0.7$ cm generates the radiation in the range from $\lambda \simeq 1$ cm to $\lambda = 10$ cm (see Fig. 4, the left graph in the middle row). If the structure period is much less than the wavelengths under consideration, only the "longwave" radiation is excited.

Let us also analyze the energy losses of the bunch by the radiation of the cylindrical waves in the area $0 < z < h$. We consider the energy passing through the lateral surface of a cylinder over the entire time. The cylinder has the radius r_0, the height h, and its axis coincides with the trajectory of the bunch motion. The energy is defined by the formula

$$W^{(2c)} = r_0 \int_{-\infty}^{+\infty} \mathrm{d}t \int_0^{2\pi} \mathrm{d}\varphi \int_0^h \mathrm{d}z S_r^{(2c)}, \tag{5.14}$$

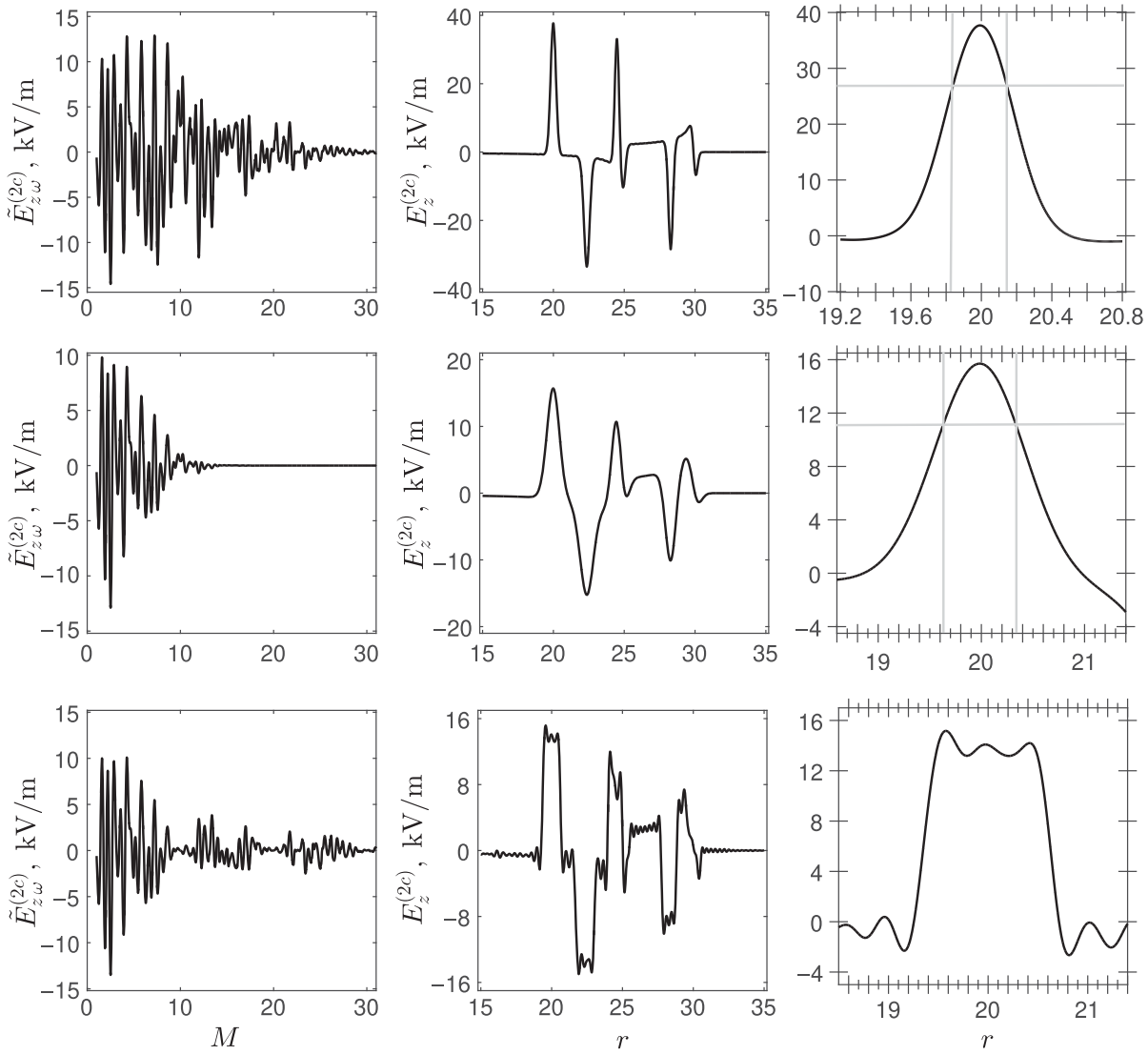


FIG. 4. Integrand $\tilde{E}^{(2c)}_{z\omega}$ depending on the integration variable M (the left column) and the electric field component $E^{(2c)}_z$ depending on the distance r (the middle and right columns) for the Gaussian (the top and middle rows) and "rectangular" (the bottom row) bunch in the case of the zeroth approximation relative to the small parameter α. The bunch parameters: $q = 1$ nC, $\beta = 0.999$, $2\sigma = 0.3$ cm (the top row), $2\sigma = 0.7$ cm (the middle row), and $2\sigma = 1$ cm (the bottom row). Other parameters: $h = 5$ cm, $z = 0$, $r = 10$ cm (the left column), $t = 1$ ns. The values of $\tilde{E}^{(2c)}_{z\omega}$ and $E^{(2c)}_z$ are given in SI units (kV/m).

where $S^{(2c)}_r = -(c/4\pi)E^{(2c)}_z H^{(2c)}_\varphi$ is the radial component of Poynting vector. Note that, due to the cylindrical symmetry of the problem, the integral over φ is equal to 2π. Then, writing the field components in the form of the Fourier integrals $F = \int_{-\infty}^{+\infty} F_\omega \exp(-i\omega t)d\omega$, substituting them into (5.14) and making some transformations, we obtain

$$W^{(2c)} = \int_0^{+\infty} \frac{dW^{(2c)}}{d\omega}\, d\omega, \tag{5.15}$$

where

$$\frac{dW^{(2c)}}{d\omega} = -2\pi c r_0 \int_0^h \mathrm{Re}[E^{(2c)}_{z\omega}(H^{(2c)}_{\varphi\omega})^*]\, dz \tag{5.16}$$

is the spectral density of the energy.

Further, we will assume that $1 < M < 2$, i.e., the distance between the grids is greater than 1 and less than 2 half-wavelengths. In this situation, the single cylindrical wave is generated (with the number $m = 1$). Substituting (5.6) into (5.16) and taking into account only the terms of

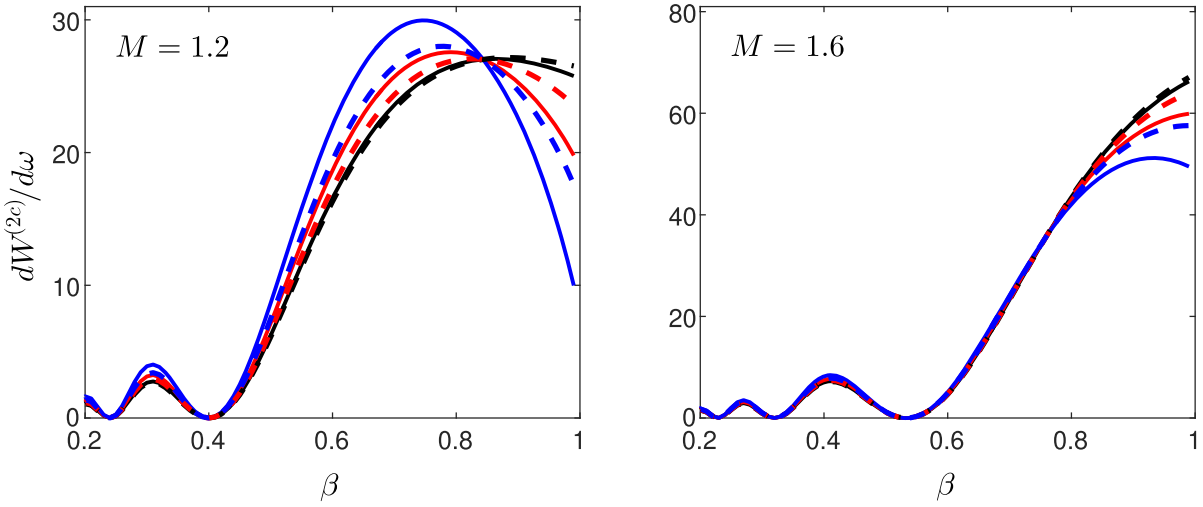


FIG. 5. Dependence of the spectral density $dW^{(2c)}/d\omega$ (in $q^2|\tilde{x}|^2/c$ units) on the bunch velocity β. The distance between the grids $h = 10$ cm, the parameter $M = 1.2$ (the wavelength $\lambda \simeq 16.7$ cm, on the left), and $M = 1.6$ (the wavelength $\lambda = 12.5$ cm, on the right). The grid period $a = 0.1$ cm (the black curves), $a = 0.5$ cm (the red curves), and $a = 1$ cm (the blue curves). The diameter of the conductors $d_0 = 0.1$ mm (the solid curves) and $d_0 = 0.5$ mm (the dashed curves).

the zeroth and first orders of smallness (relative to α), we obtain

$$\frac{dW^{(2c)}}{d\omega} \simeq 16\pi \frac{q^2|\tilde{x}|^2\beta^2}{c} \frac{M(M^2-1)}{(M^2-\beta^2)^2}\left[1+\cos\left(\frac{\pi M}{\beta}\right)\right] \times\left\{1+2\alpha A\left[\frac{5-2M^2+M^4}{M^2-1}-\frac{4\beta^2(M^2+1)}{M^2-\beta^2}\right]\right\}. \tag{5.17}$$

Figure 5 demonstrates the dependence of the spectral density $dW^{(2c)}/d\omega$ (in $q^2|\tilde{x}|^2/c$ units) on the bunch velocity β for different values of the parameter M, the grid period a, and the thickness of the wires, d_0. As one can see, the dependencies are characterized by a number of extreme values due to the function $\cos(\pi M/\beta)$ in (5.17). Note that, in the range of relatively large bunch velocities, the energy losses are greatest, and the spectral density varies significantly with changes in the grid parameters. According to the graphs, an increase in β results in a maximum with a relatively large magnitude (the main maximum) or a monotonic increase of the spectral density. It depends, in particular, on the parameter M, which can vary from 1 to 2. As the calculations show, with increasing M the dependence becomes monotonic, and the range of β under consideration decreases. In the case when there is the main maximum, the bunch velocity corresponding to the maximal value of the spectral density increases with a decrease in a as well as with an increase in d_0 and M. For example, if $a = 1$ cm and $d_0 = 0.1$ mm (the solid blue curves), β is approximately equal to 0.75 for $M = 1.2$ (on the left) and 0.93 for $M = 1.6$ (on the right). It should be mentioned that, for the bunch velocities close to 1, the dependence of the spectral density on a and d_0 is always clear: it increases with a decrease of the grid period and an increase of the wire thickness. We note as well that, for any bunch velocity, the dependence of $dW^{(2c)}/d\omega$ on d_0 is weaker than the dependence on a.

Finally, we compare the results presented here for the cylindrical waves with the ones of a classical problem concerning the radiation of a charge passing through the single ideal screen [25] (we note that a perfectly conductive solid surface is meant by this term). As is known, the Fourier transform of the magnetic field generated in the area between the grids is determined by (5.6). Assuming that $1 < M < 2$ ($m = 1$) and taking into account the linear approximation relative to α, we can write the absolute value of $H^{(2c)}_{\varphi\omega}$ as follows

$$|H^{(2c)}_{\varphi\omega}| \simeq \frac{4q|\tilde{x}|\beta}{c\sqrt{hr}} \times\frac{M(M^2-1)^{1/4}}{M^2-\beta^2}\sqrt{1+\cos\left(\frac{\pi M}{\beta}\right)} \times\left\{1+\alpha A\left[\frac{2M^4-3(M^2-1)}{M^2-1}-4\beta^2\frac{M^2+1}{M^2-\beta^2}\right]\right\}. \tag{5.18}$$

Note that (5.18) describes the Fourier transform of the magnetic field under the condition $\theta = \pi/2$.

The corresponding component in the case of the single ideal screen, located at $z = 0$, is given by [25]

$$H^{id}_{\varphi\omega} \simeq \frac{2q\tilde{x}\beta}{c}\frac{\sin\theta}{1-\beta^2\cos^2\theta}\frac{\exp(ik_0R)}{R}. \tag{5.19}$$

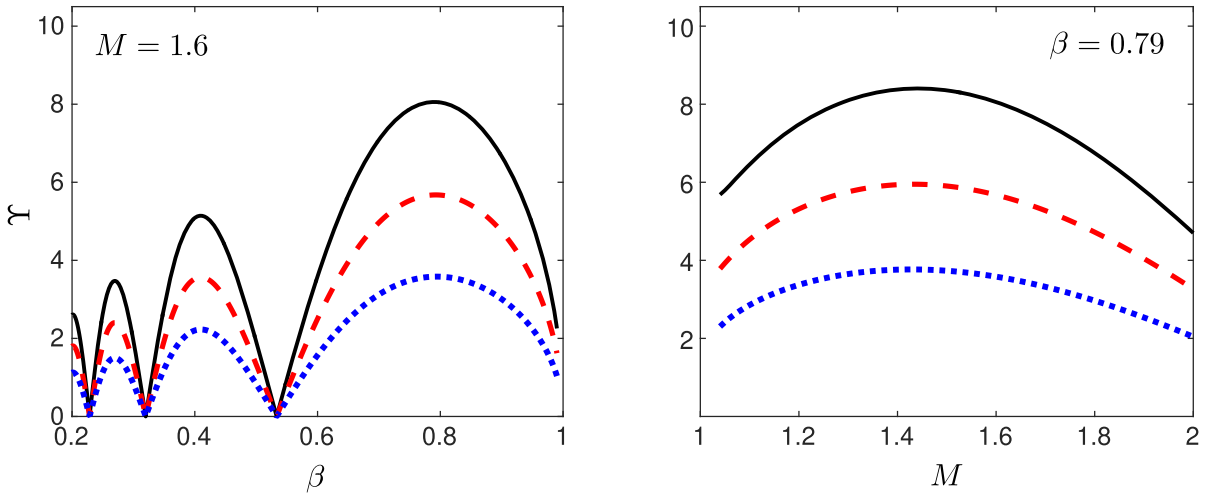


FIG. 6. Dependence of Υ on the bunch velocity β (on the left) and the parameter M (on the right). The distance between the grids $h = 1$ cm (the solid black curves), $h = 2$ cm (the dashed red curves), and $h = 5$ cm (the dotted blue curves). The distance $R = 10$ cm. The grid period $a = 0.1$ cm, the diameter of the conductors $d_0 = 0.1$ mm. The values of M and β are given in the figure.

It is easy to show that (5.19) has the maximal value in the direction

$$\theta = \theta_{\max} = \arcsin\left(\sqrt{1-\beta^2}/\beta\right). \tag{5.20}$$

According to this equation, $\theta_{\max}$ is equal to $\pi/2$, if $\beta \le 1/\sqrt{2} \simeq 0.71$, and decreases to zero with an increase of the velocity from $1/\sqrt{2}$ to 1. In the direction $\theta = \theta_{\max}$, the absolute value of (5.19) is determined by the formula

$$|(H^{id}_{\varphi\omega})_{\max}| = \frac{q|\tilde{x}|}{cR\sqrt{1-\beta^2}}. \tag{5.21}$$

It is of interest to compare expressions (5.18) and (5.21) under the condition that an observation point is located at the same distance from the origin, i.e., when $r = R$. Figure 6 demonstrates the dependence of $\Upsilon = |H^{(2c)}_{\varphi\omega}|/|(H^{id}_{\varphi\omega})_{\max}|$ on the bunch velocity β and the parameter M. The value of β, at which Υ has the main maximum (on the left), was used to obtain the dependence on M (on the right). The distance between the grids, h, is equal to 1 cm (the solid black curves), 2 cm (the dashed red curves), and 5 cm (the dotted blue curves). As shown in Fig. 6, the intensity of the radiation considered can be significantly greater than the one in the case of the single ideal screen. In particular, the maximum value of Υ is approximately equal to 8.4 under condition that $h = 1$ cm, $\beta \simeq 0.79$, and $M \simeq 1.44$ (the wavelength $\lambda \simeq 1.39$ cm).

Note that the value of Υ can be increased by a decrease of h, which is illustrated in Fig. 6, and an increase of the distance R. This is clear from (5.18) and (5.21): $\Upsilon \propto \sqrt{R/h}$. However, the range of h under consideration is limited due to the problem formulation (2.1), that is, the distance between the grids has to be relatively large compared to the grid period a. It should also be emphasized that the value of Υ increases with decreasing a and increasing the wire diameter d_0, but these dependencies are relatively weak.

We note again that the electromagnetic radiation generated in the area between the grid structures propagates in the direction perpendicular to that of the bunch motion. Due to this fact, one can place a detector in such a way as to minimize the influence of a bunch on the device. This can be another advantage of the structure under consideration over the single ideal screen. Especially, this is obvious in the case of ultrarelativistic bunch velocities, when the direction of the radiation from the single ideal screen is almost parallel to the trajectory of bunch motion.

It should also be added that the electromagnetic waves under investigation can be observed in an experiment, in particular, using a wideband antenna [27,28], which is sensitive to wavelengths corresponding to tens of millimeters. As was shown above, the characteristics of the radiation can be changed for the effective detection. For example, the lengths of the electromagnetic waves can be decreased by a decrease of the distance between the grids.

VI. CONCLUSION

We investigated the electromagnetic radiation of a thin charged particle bunch passing through two parallel grids with square cells. It was assumed that the distance between the grids and the wavelengths under consideration are much greater than the cell size, and the latter is much greater than the thickness of the wires that form each grid and have galvanic contact at the cross points. These assumptions allowed us to apply the ABC method and obtain the analytical solution of the problem.

It was demonstrated that the radiation field generated by the bunch consists of spherical and cylindrical waves. As was shown, the spherical ones are dominant outside the area between the grids. The electromagnetic field of the wave differs from that in the case of a single ideal screen due to the corrections proportional to the small parameter of the problem. In the area between the grids, the spherical waves can be neglected at the relatively great distance from the trajectory of the bunch motion, and the cylindrical waves are dominant in this area. A number of propagating modes depends on the relation between the half-wavelength and the distance between the grids. In particular, if the distance is greater than 1 and less than 2 half-wavelengths, the single mode is generated. Outside the area between the grids, the cylindrical waves are also excited, but each mode exists in a certain range of angles and has a relatively small magnitude. We showed as well that the electromagnetic field of the cylindrical waves excited in the area between the grids can be used for determining the bunch parameters, such as the length and longitudinal shape.

It should be emphasized that the double screen composed of parallel grids with square cells has a series of advantages over the single ideal screen as well as the SEM grids [21–24], which are used for bunch diagnostics. In particular, the structure under consideration can be practically transparent to a bunch due to the fact that the grid properties depend little on the wire thickness, and the latter can be greatly reduced. The electromagnetic field generated between the grids can be significantly more intense than that of a single ideal screen, and the bunch parameters can be determined by analyzing the structure of this field. Another considerable advantage is that a measuring device can be positioned perpendicular to the direction of bunch motion. This is especially important in the case of ultrarelativistic bunches, i.e., when the maximum intensity of transition radiation from a solid conductive surface (for example, a foil) is observed in the direction, which is almost parallel to the trajectory of bunch motion. Thus, the double grid screen can be considered a quite promising tool for generating electromagnetic radiation and nondestructive bunch diagnostics.

DATA AVAILABILITY

The data that support the findings of this article are not publicly available. The data are available from the authors upon reasonable request.

[1] S. J. Smith and E. M. Purcell, Visible light from localized surface charges moving across a grating, Phys. Rev. Lett. **92**, 1069 (1953).

[2] A. P. Potylitsyn, M. I. Ryazanov, M. N. Strikhanov, and A. A. Tishchenko, *Diffraction Radiation from Relativistic Particles*, Springer Tracks in Modern Physics (Springer Berlin, Heidelberg, Berlin, 2011), Vol. 239, 10.1007/978-3-642-12513-3.

[3] A. P. Potylitsyn, *Electromagnetic Radiation of Electrons in Periodic Structures*, Springer Tracks in Modern Physics (Springer Berlin, Heidelberg, Berlin, 2011), Vol. 243, 10.1007/978-3-642-19248-7.

[4] D. Y. Sergeeva, A. A. Tishchenko, and M. N. Strikhanov, Conical diffraction effect in optical and x-ray Smith-Purcell radiation, Phys. Rev. ST Accel. Beams **18**, 052801 (2015).

[5] G. A. Naumenko, A. P. Potylitsyn, D. Y. Sergeeva, A. A. Tishchenko, M. N. Strikhanov, and V. V. Bleko, First experimental observation of the conical effect in Smith-Purcell radiation, JETP Lett. **105**, 553 (2017).

[6] J. M. Wachtel, Free-electron lasers using the Smith-Purcell effect, J. Appl. Phys. **50**, 49 (1979).

[7] H. L. Andrews, C. A. Brau, J. D. Jarvis, C. F. Guertin, A. O'Donnell, B. Durant, T. H. Lowell, and M. R. Mross, Observation of THz evanescent waves in a Smith-Purcell free-electron laser, Phys. Rev. ST Accel. Beams **12**, 080703 (2009).

[8] G. Doucas, M. F. Kimmitt, A. Doria, G. P. Gallerano, E. Giovenale, G. Messina, H. L. Andrews, and J. H. Brownell, Determination of longitudinal bunch shape by means of coherent Smith-Purcell radiation, Phys. Rev. ST Accel. Beams **5**, 072802 (2002).

[9] G. Doucas, V. Blackmore, B. Ottewell, C. Perry, P. G. Huggard, E. Castro-Camus, M. B. Johnston, J. Lloyd-Hughes, M. F. Kimmitt, B. Redlich, and A. van der Meer, Longitudinal electron bunch profile diagnostics at 45 MeV using coherent Smith-Purcell radiation, Phys. Rev. ST Accel. Beams **9**, 092801 (2006).

[10] K. L. F. Bane and G. Stupakov, Terahertz radiation from a pipe with small corrugations, Nucl. Instrum. Methods Phys. Res., Sect. A **677**, 67 (2012).

[11] K. Bane, G. Stupakov, S. Antipov, M. Fedurin, K. Kusche, C. Swinson, and D. Xiang, Measurements of terahertz radiation generated using a metallic, corrugated pipe, Nucl. Instrum. Methods Phys. Res., Sect. A **844**, 121 (2017).

[12] E. S. Simakov, A. V. Tyukhtin, and S. N. Galyamin, Radiation of a charge moving along a corrugated surface with a relatively small period, Phys. Rev. Accel. Beams **22**, 061301 (2019).

[13] E. S. Simakov and A. V. Tyukhtin, Radiation of a charged particle bunch moving along a deeply corrugated structure with a relatively small period, Nucl. Instrum. Methods Phys. Res., Sect. A **1028**, 166387 (2022).

[14] E. I. Nefedov and A. N. Sivov, *Elektrodinamika Periodicheskih Struktur* (Nauka, Moskva, 1977).

[15] M. I. Kontorovich, M. I. Astrakhan, V. P. Akimov, and G. A. Fersman, *Elektrodinamika Setchatyh Struktur* (Radio i Sviaz, Moskva, 1987).

[16] A. V. Tyukhtin, V. V. Vorobev, and S. N. Galyamin, Radiation excited by a charged-particle bunch on a planar periodic wire structure, Phys. Rev. ST Accel. Beams **17**, 122802 (2014).

[17] A. V. Tyukhtin, V. V. Vorobev, and S. N. Galyamin, Radiation of charged-particle bunches passing perpendicularly by the edge of a semi-infinite planar wire structure, Phys. Rev. E **91**, 063202 (2015).

[18] V. V. Vorobev, A. V. Tyukhtin, and S. N. Galyamin, Surface waves generated by charged particle bunch moving along the edge of semi-infinite planar wire grid, Radiat. Phys. Chem. **133**, 91 (2017).

[19] E. G. Doil'nitsina and A. V. Tyukhtin, Selective screening of waveguide modes by a system of two grids with square cells, J. Commun. Technol. Electron. **54**, 1171 (2009).

[20] A. V. Tyukhtin, Method of particle energy determination based on measurement of waveguide mode frequencies, J. Phys. Conf. Ser. **357**, 012003 (2012).

[21] M. Plum, Interceptive beam diagnostics-signal creation and materials interactions, AIP Conf. Proc. **732**, 23 (2004).

[22] U. Raich, Beam diagnostics, in *Proceedings of the CAS-CERN Accelerator School: Ion Sources* (CERN, Geneva, 2013), p. 503, 10.5170/CERN-2013-007.503.

[23] P. Forck, *Lecture Notes on Beam Instrumentation and Diagnostics*, Joint Universities Accelerator School (JUAS), GSI, Darmstadt, Germany (2018), https://indico.cern.ch/event/683638/contributions/2801669/attachments/1563566/2540684/juas_script.pdf.

[24] P. Forck, Beam instrumentation, in *Proceedings of the Joint Universities Accelerator School (JUAS): Courses and Exercises* (CERN, Geneva, 2024), p. 1339, 10.23730/CYRSP-2024-003.1339.

[25] V. L. Ginzburg and V. N. Tsytovich, *Perekhodnoe Izluchenie i Perekhodnoe Rasseyanie* (Nauka, Moskva, 1984).

[26] L. B. Felsen and N. Marcuvitz, *Radiation and Scattering of Waves* (Prentice-Hall, New Jersey, 1973).

[27] A. Aleinik, A. Aryshev, B. Kalinin, G. Naumenko, A. Potylitsyn, G. Saruev, A. Sharafutdinov, O. Malakhovskii, and E. Monastyrev, Coherent diffraction radiation of a 6-MeV microtron electron beam, JETP Lett. **76**, 337 (2002).

[28] B. Kalinin, G. Naumenko, A. Potylitsyn, G. Saruev, L. Sukhikh, and V. Cha, Measurement of the angular characteristics of transition radiation in near and far zones, JETP Lett. **84**, 110 (2006).